Dioxygen Activation by a Dinuclear Thiolate-ligated Fe(II) Complex

*Chang-Chih Hsieh,[a] Yu-Chiao Liu,[b] Mei-Chun Tseng,[b] Ming-Hsi Chiang[b] and Yih-Chern Horng[a]**

[a.] Department of Chemistry, National Changhua University of Education, Changhua 50058, Taiwan

[b.] Institute of Chemistry, Academia Sinica, Taipei 11528, Taiwan, Republic of China

Electronic Supporting Information

Table of Contents

Supplementary Tables and Figures

Table S0. The summary of crystallographic data for complexes and organic ligands.

	Complex **1**	Complex **2** · H2O	$(LNHS)_2$	LN-S
formula	C52H44Fe2N8O4S4	C34H42FeN5O3S2	C26H22N4O2S2	C13H10N2OS
fw	1084.89	688.70	486.60	242.30
temp, K	150(2)	150(2)	296(2) K	296(2) K
cryst syst	Monoclinic	Monoclinic	Monoclinic	Monoclinic
space group	*P2(1)/n*	*P2(1)/c*	*P2(1)/n*	*P2(1)/c*
a, Å	11.1144(6)	15.879(3)	7.8144(4)	9.9938(16)
b, Å	15.7599(7)	12.862(3)	19.0194(9)	13.994(2)
c, Å	14.9052(7)	16.892(3)	15.7767(7)	8.1879(13)
α, º	90	90	90	90
β, °	105.382(3)	102.985(14)	95.996(3)	97.361(11)
γ, º	90	90	90	90
Volume, $Å^3$ / *Z*	2517.3(2)/2	3361.8(11)/4	2331.99(19)/4	1135.7(3)/4
Density (cald.), Mg/m^3	1.431	1.361	1.386	1.417
Absorption coefficient, mm^{-1}	0.796	0.615	0.261	0.267
crystal size, mm	0.25 x 0.16 x 0.07	0.17 x 0.07 x 0.05	0.27 x 0.08 x 0.08	0.32 x 0.11 x 0.11
θ range, deg	1.92 to 28.72	2.01 to 24.50	1.68 to 28.28	2.05 to 28.79
no. of reflns collected	29928	31974	34428	13677
no. of indep reflns	6489	5583	5720	2935
max. and min. trans	0.940 and 0.852	0.960 and 0.940	0.979 and 0.933	0.952 and 0.944
no. of data /restraints /params	6489 / 0 / 324	5583 / 3 / 418	5720 / 0 /307	2935 / 0 / 154
goodness-of-fit on F^2	0.789	0.937	0.866	0.985
final *R* indices	0.0350	0.0629	0.0533	0.0389
$[I>2\sigma(I)]$ R_1[a], wR_2[b]	0.1019	0.1419	0.1274	0.1295
R indices (all data),	0.0539	0.1547	0.1514	0.0541
R_1[a] ,wR_2[b]	0.1213	0.2051	0.1768	0.1428
largest diff. peak and hole, e $Å^{-3}$	0.377 and -0.373	0.302 and -0.365	0.194 and -0.223	0.163 and -0.307

[a] $R_1 = \Sigma \mid F_0 \mid - \mid F_c \mid / \Sigma \mid F_0 \mid$

[b] $wR_2 = [\Sigma[\omega(F_0^2 - F_c^2)^2] / \Sigma[\omega(F_0^2)^2]]^{1/2}$

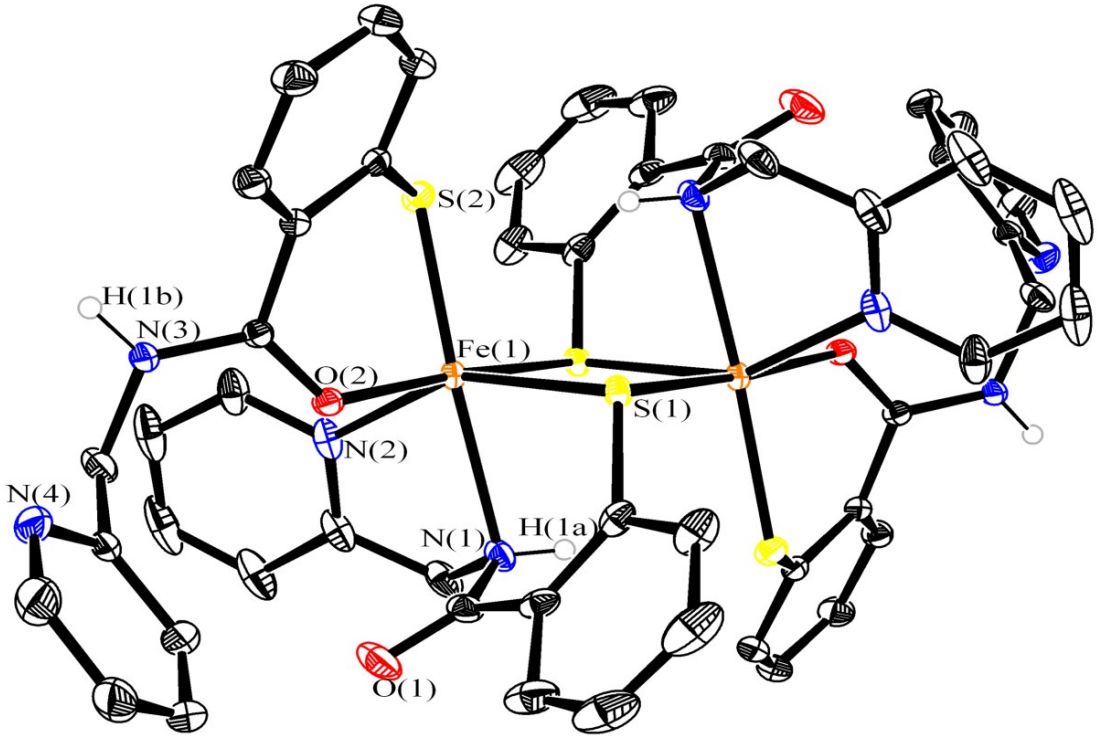

Table S1. Selected bond lengths (Å) and angles (º) for complex **1**[a]

Fe(1)- Fe(1)A	3.5477(4)	S(1)-Fe(1)-O(2)	94.35(4)
Fe(1)-S(1)	2.4451(6)	S(2)-Fe(1)-S(1)A	94.477(19)
Fe(1)-S(1)A	2.5306(5)	S(2)-Fe(1)-N(1)	174.53(5)
Fe(1)-S(2)	2.3555(6)	S(2)-Fe(1)-N(2)	106.80(6)
Fe(1)-N(1)	2.45020(20)	S(2)-Fe(1)-O(2)	89.64(4)
Fe(1)-N(2)	2.1430(18)	N(1)-Fe(1)-S(1)A	80.07(5)
Fe(1)-O(2)	2.1788(14)	N(1)-Fe(1)-N(2)	73.43(7)
S(1)-S(1)A	3.4899(6)	N(1)-Fe(1)-O(2)	95.78(6)
S(1)-Fe(1)-S(2)	101.25(2)	N(2)-Fe(1)-S(1)A	93.28(5)
S(1)-Fe(1)-S(1)A	89.060(18)	N(2)-Fe(1)-O(2)	81.41(6)
S(1)-Fe(1)-N(1)	79.11(5)	O(2)-Fe(1)-S(1)A	174.05(4)
S(1)-Fe(1)-N(2)	151.57(6)	Fe(1)-S(1)-Fe(1)A	90.941(18)

[a] Symmetry transformations used to generate equivalent atoms: A: 1 -x+1,-y,-z+1.

Table S2. Collected bond lengths (Å) and angles (°) for complexes with similar Fe^{II}-Fe^{II}(μ-SR)$_2$ cores

Metal complex	Fe-Fe	S-S	Fe-S	Fe-S	Fe-S[a]	Fe-S-Fe	S-Fe-S	C. N.
(μ-S,S)[Fe(L^{AP})$_2$]$_2$[1]	2.919	3.799[b]	2.397	2.394	2.396	75.07[b]	104.93[b]	5
[(bme*-daco)Fe]$_2$[2]	3.31	3.595[b]	2.444	2.441	2.443	85.24[b]	94.76[b]	5
[(bme-daco)Fe]$_2$[3]	3.217[b]	3.611[b]	2.421	2.417	2.419	83.4	96.6	5
[Fe($C_8H_{18}N_2S_2$)]$_2$[4]	3.206	3.558	2.471	2.379	2.425	82.68[b]	97.32[b]	5
[Fe($C_9H_{20}N_2S_2$)]$_2$[4]	3.371	3.641	2.490	2.411	2.451	86.91[b]	93.09[b]	5
[Fe('$N_2H_2S_3$')]$_2$[5]	3.340[b]	3.673[b]	2.517	2.447	2.482	84.57[b]	95.43[b]	6
[Fe($pyCO_2MeS_4$)]$_2$[6]	3.391[b]	3.146[b]	2.348	2.277	2.313	94.28[b]	85.72[b]	6
Complex **1**	3.548	3.490	2.531	2.445	2.488	90.94	89.06	6

[a] Averaged of bond lengths or angles. [b] The data were measured by Mercury 3.5.1 software.

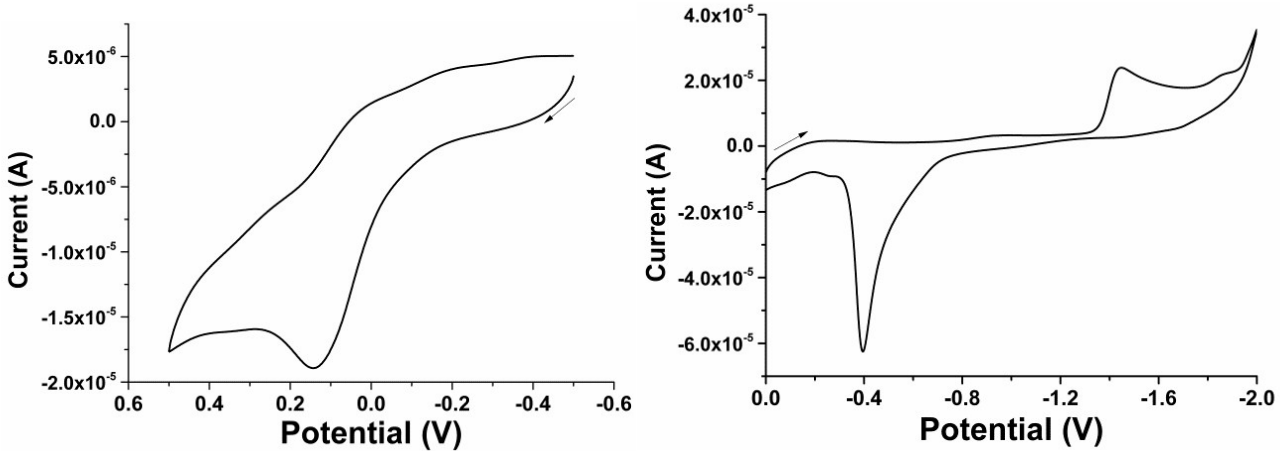

Figure S1. Cyclic voltammetry analyses of **1** (1 mM) at RT, scan rate 0.05 V/s.

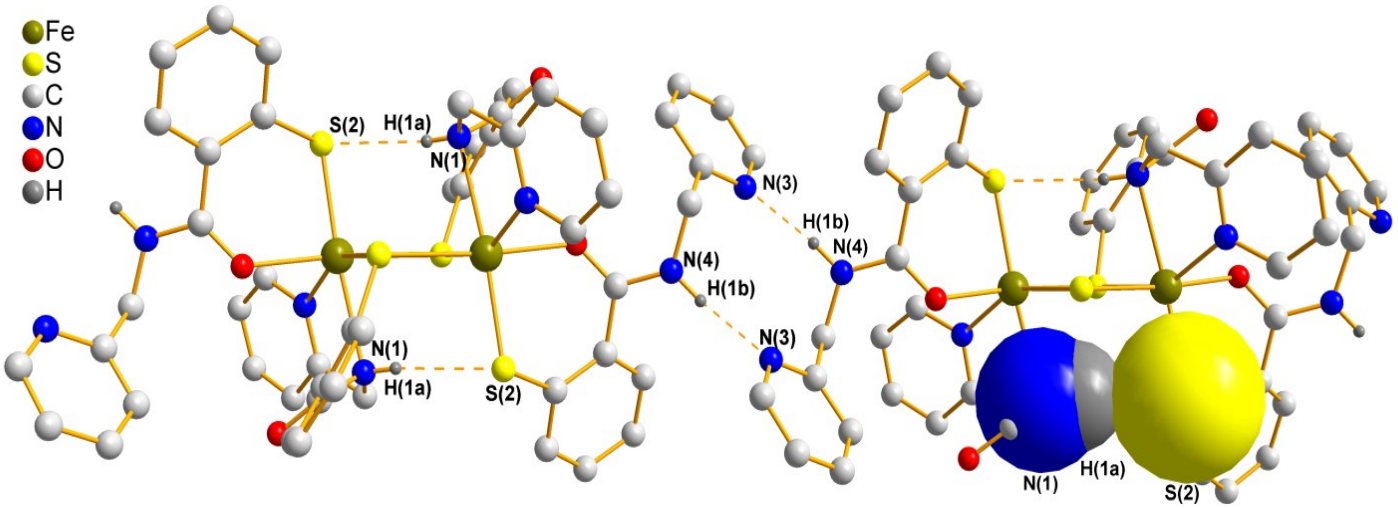

Figure S2. Packing diagrams of complex **1** with NH···S intramolecular (N···S: 3.379 Å, NH···S: 2.587 Å and ∠NH···S: 173.37°) and NH···N intermolecular (N···N: 2.911 Å, NH···N: 2.034 Å and ∠NH···N: 163.56°) hydrogen bond interactions. The space-fill drawings of NH···S intramolecular hydrogen bond interactions are shown in the right molecule. Some carbon atoms are omitted for clarity.

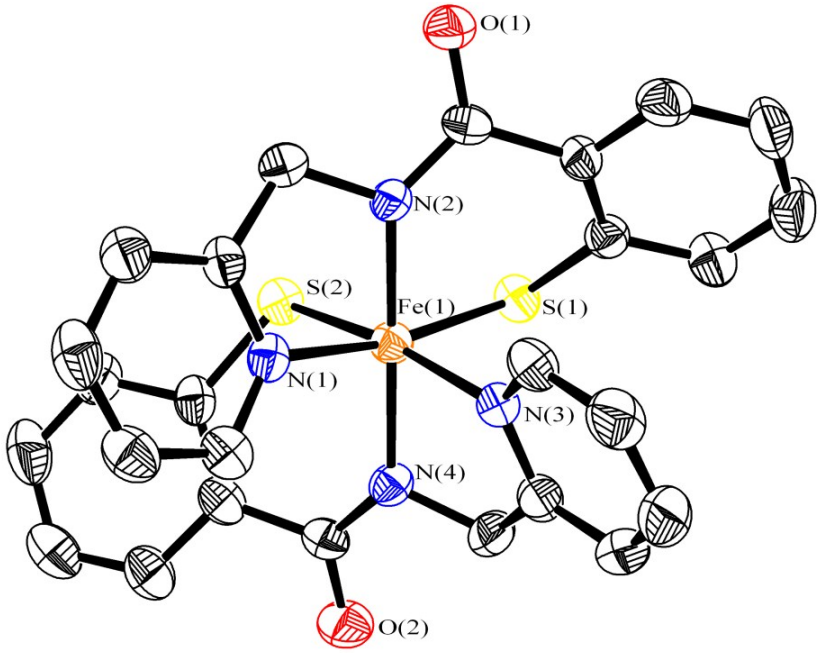

Table S3. Selected bond lengths (Å) and angles (º) for complex **2**

Fe(1)-S(1)	2.265(2)	S(2)-Fe(1)-N(1)	89.78(15)
Fe(1)-S(2)	2.265(2)	S(2)-Fe(1)-N(2)	93.24(16)
Fe(1)-N(1)	2.018(5)	S(2)-Fe(1)-N(3)	171.26(17)
Fe(1)-N(2)	1.942(5)	S(2)-Fe(1)-N(4)	90.77(17)
Fe(1)-N(3)	2.002(5)	N(1)-Fe(1)-N(2)	79.8(2)
Fe(1)-N(4)	1.949(5)	N(1)-Fe(1)-N(3)	92.0(2)
S(1)-Fe(1)-S(2)	89.15(7)	N(1)-Fe(1)-N(4)	96.4(2)
S(1)-Fe(1)-N(1)	170.11(17)	N(2)-Fe(1)-N(3)	95.5(2)
S(1)-Fe(1)-N(2)	90.45(16)	N(2)-Fe(1)-N(4)	174.4(2)
S(1)-Fe(1)-N(3)	90.59(16)	N(3)-Fe(1)-N(4)	80.5(2)
S(1)-Fe(1)-N(4)	93.45(16)		

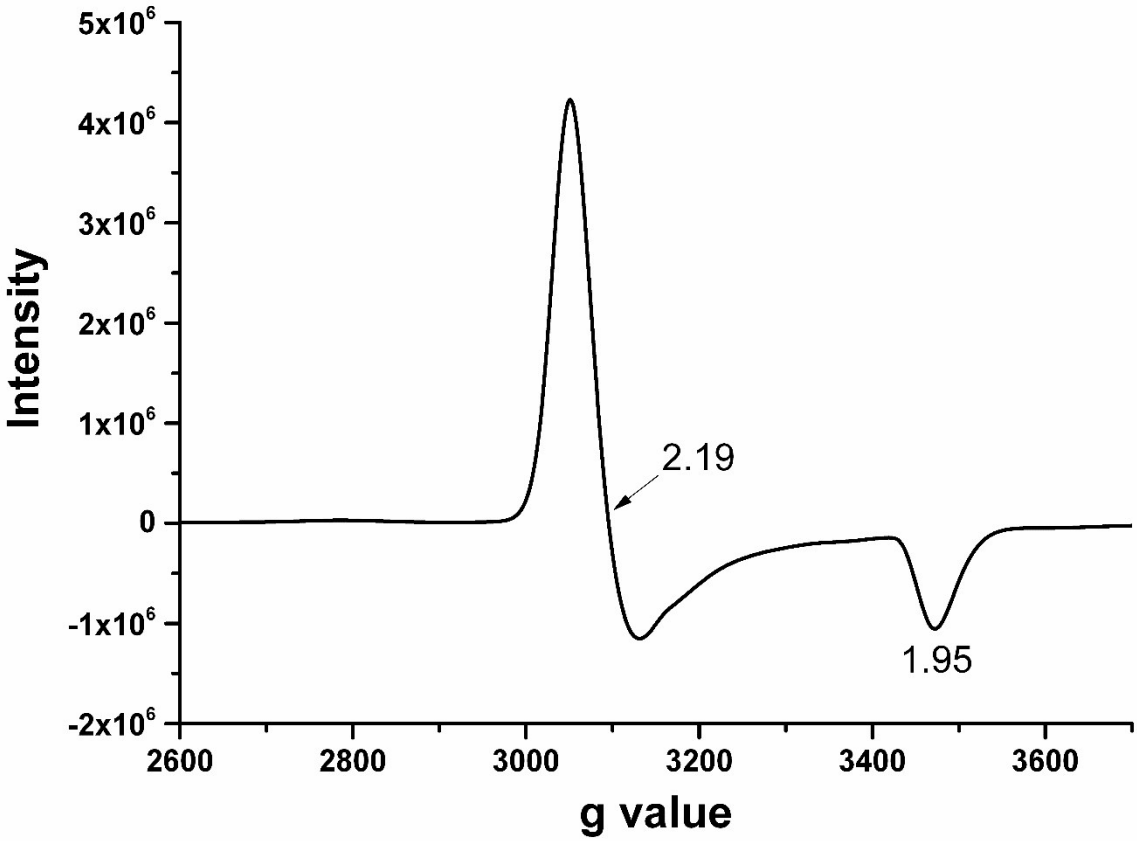

Figure S3. EPR spectrum of complex **2** in 50% DMSO aqueous solution measured at 77 K. Spectrometer settings: microwave frequency, 9.5 GHz; modulation frequency, 100 kHz; modulation amplitude, 10 G; time constant, 655.36 msec; conversion time, 20.48 msec; microwave power, 0.632 mW; receiver gain, 5.02×10^3.

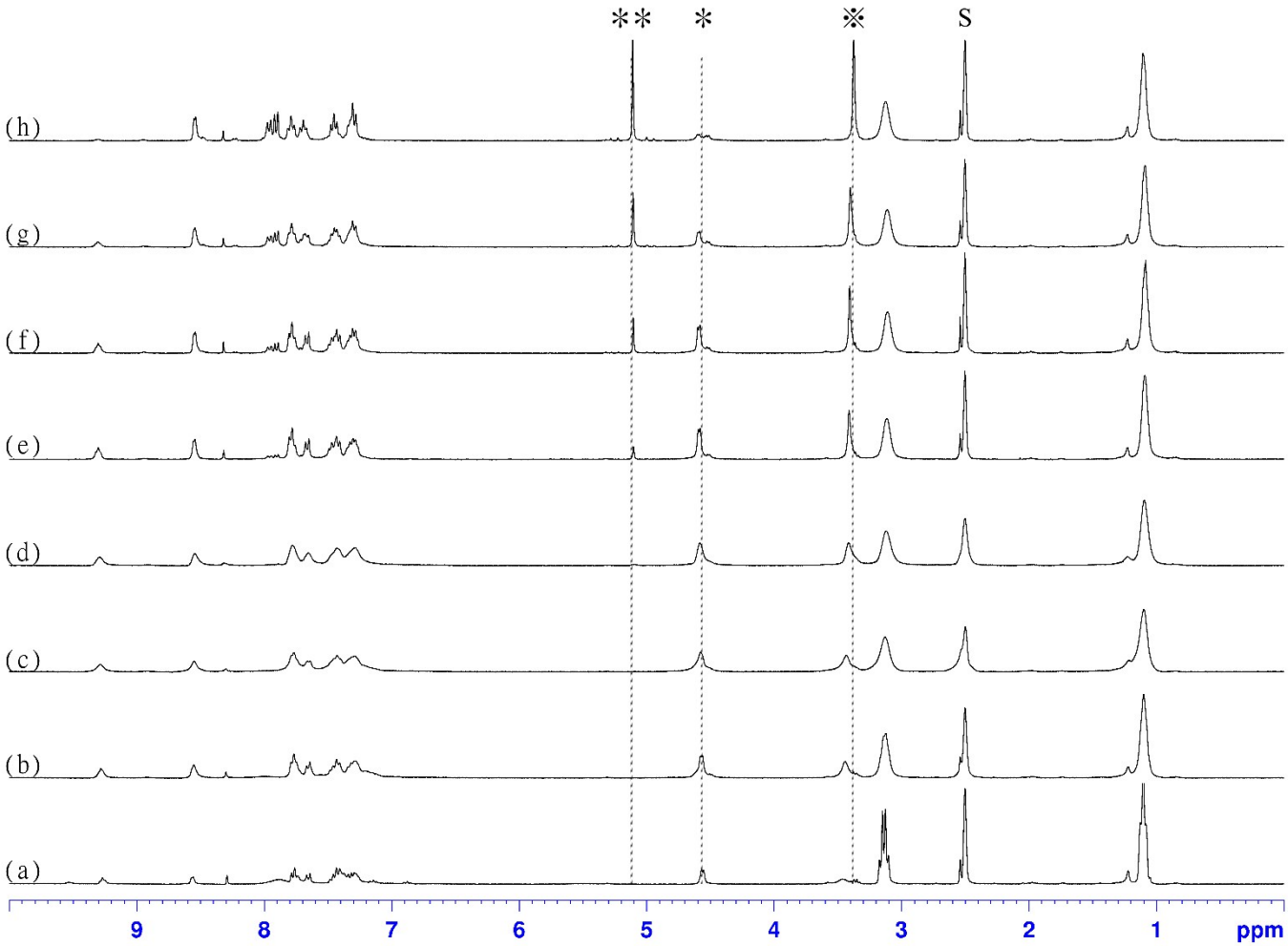

Figure S4 Time-dependent ^{1}H NMR spectra in d_6-DMSO (S) of (a) the solution containing pure **1** and one equiv $(LNHS)_2$ in N_2(g), (b) after addition of oxygen for 10 mins, (c) for 25 mins, (d) for 2 h, (e) for 6 h, (f) for 11 h, (g) for 1 day, and (h) for 2 days. The chemical shifts of CH_2 (*) in $(LNHS)_2$, CH_2 (**) in LN-S, and H_2O (※) are marked.

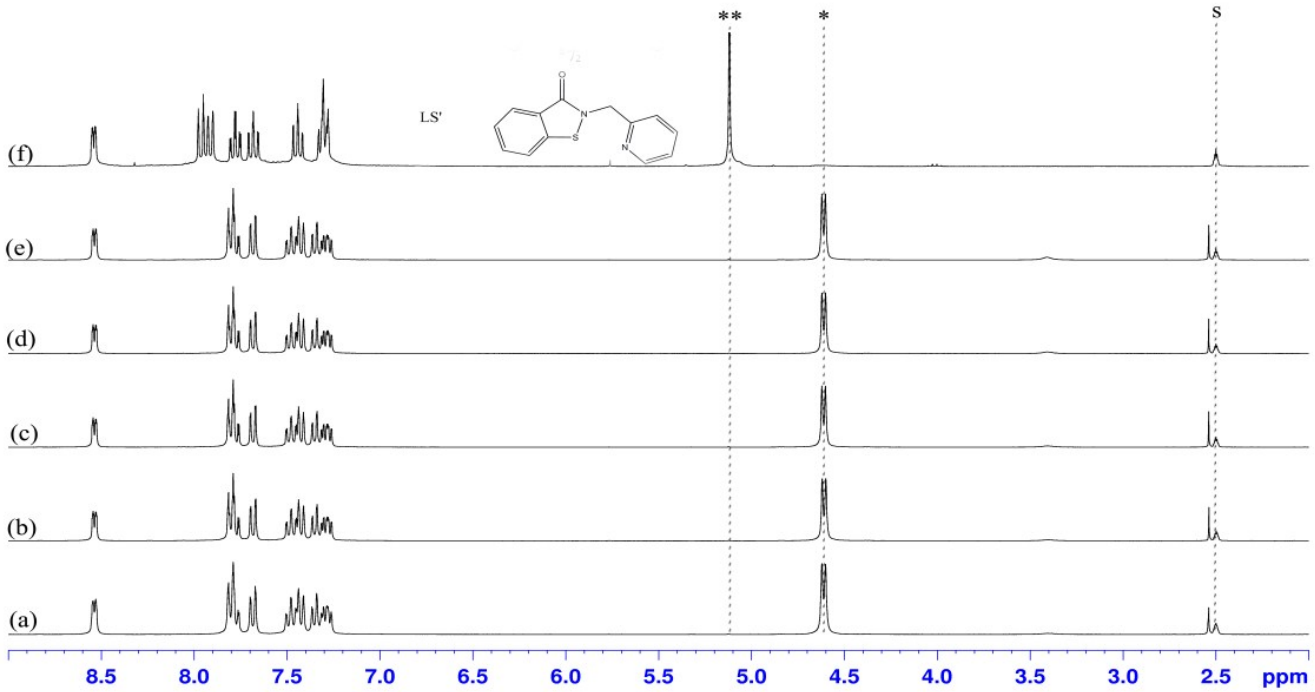

Figure S5. ^{1}H NMR spectra (300 MHz, 298 K, d_6-DMSO (S)) of pure $(LNHS)_2$ in air for (a) 0 day, (b) 1 days, (c) 2 days;, (d) 3 days, (e) 4 days, and (f) of pure LN-S. The chemical shifts of CH_2 (*) in $(LNHS)_2$ and CH_2 (**) in LN-S are indicated. LN-S was not generated from the solution of $(LNHS)_2$ in DMSO for 5 days in air.

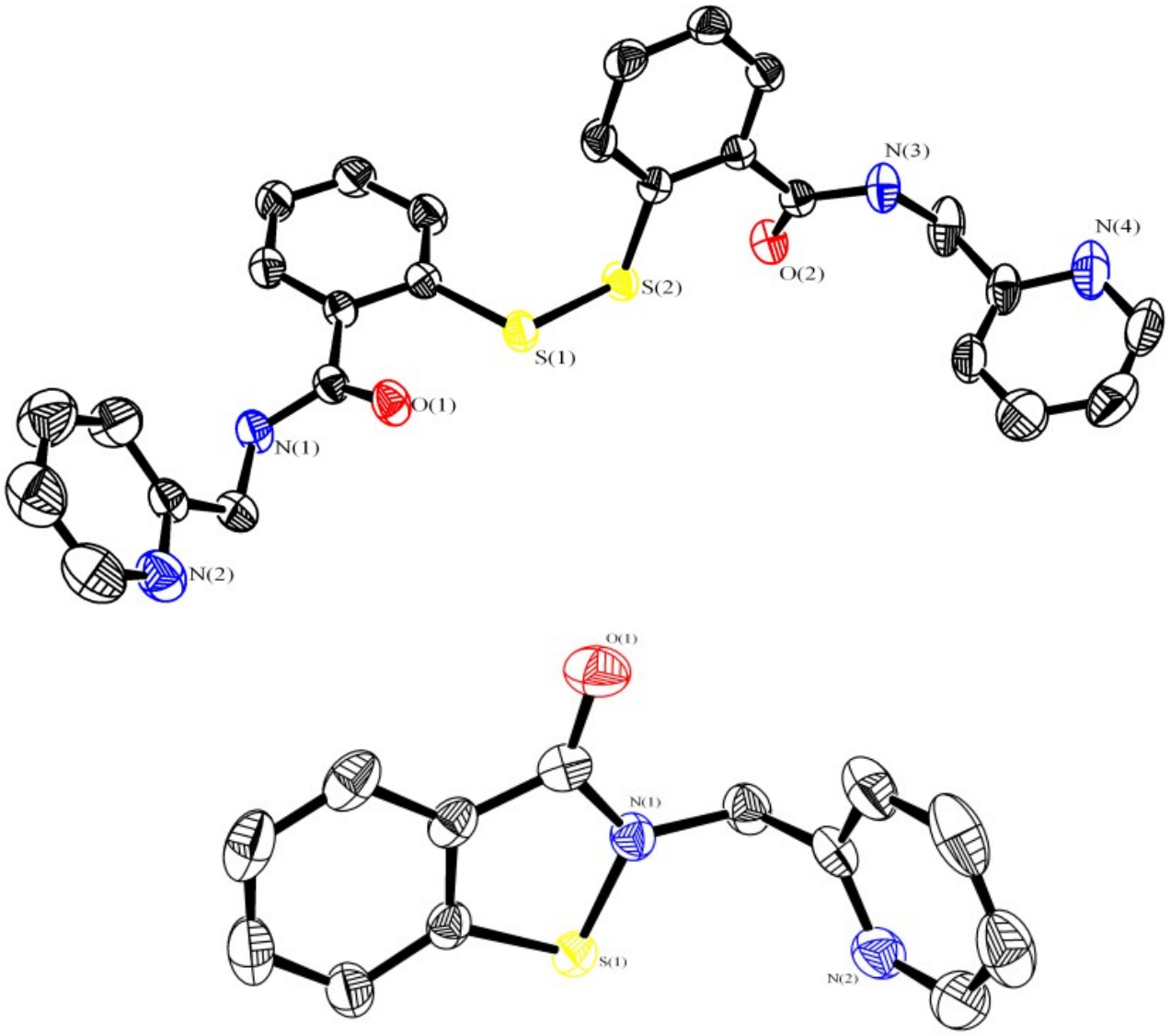

Figure S6. ORTEP drawings of $(LNHS)_2$ (Top) and LN-S (Bottom). The thermal ellipsoids are drawn at the 35% probability level. Hydrogen atoms are omitted for clarity.

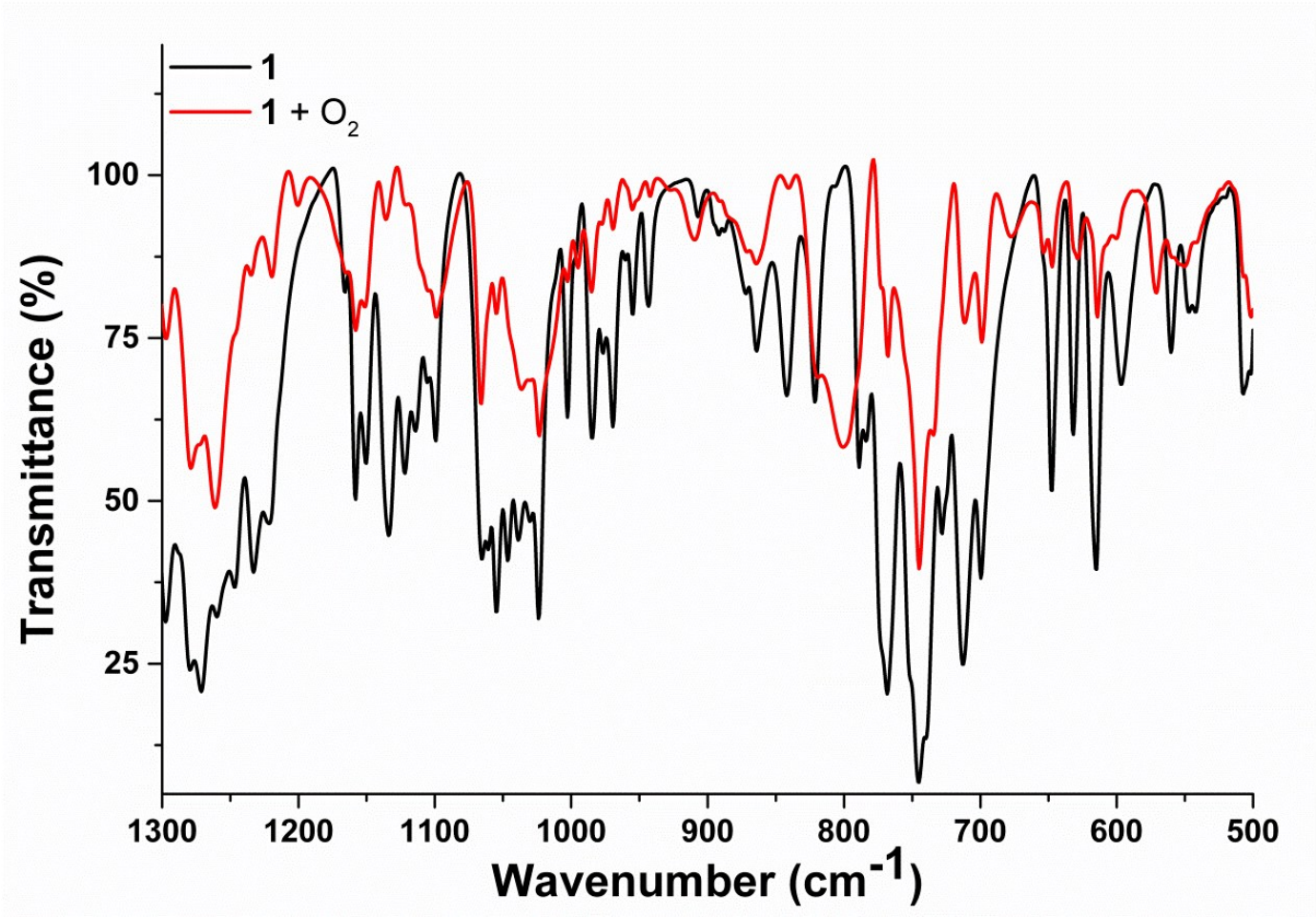

Figure S7. Solid IR spectra of complex **1** and oxygenated complex **1** (the preparation of oxygenated complex **1** was described in the experimental section).

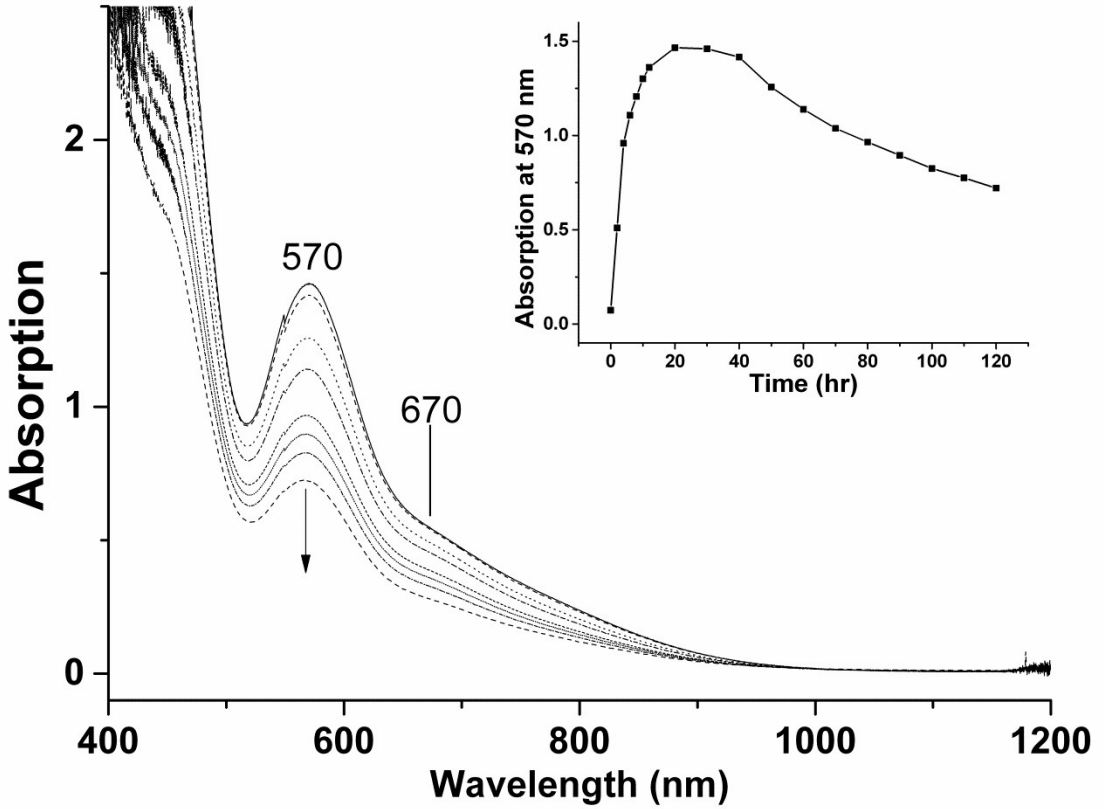

Figure S8. UV-vis spectral changes of the decaying Fe^{III}-O_2-Fe^{III} intermediate for the reaction of **1** with limited excess O_2 in DMSO at RT. The inset shows the time-dependent formation and degradation of the Fe^{III}-O_2-Fe^{III} intermediate by following the absorption band at 570 nm.

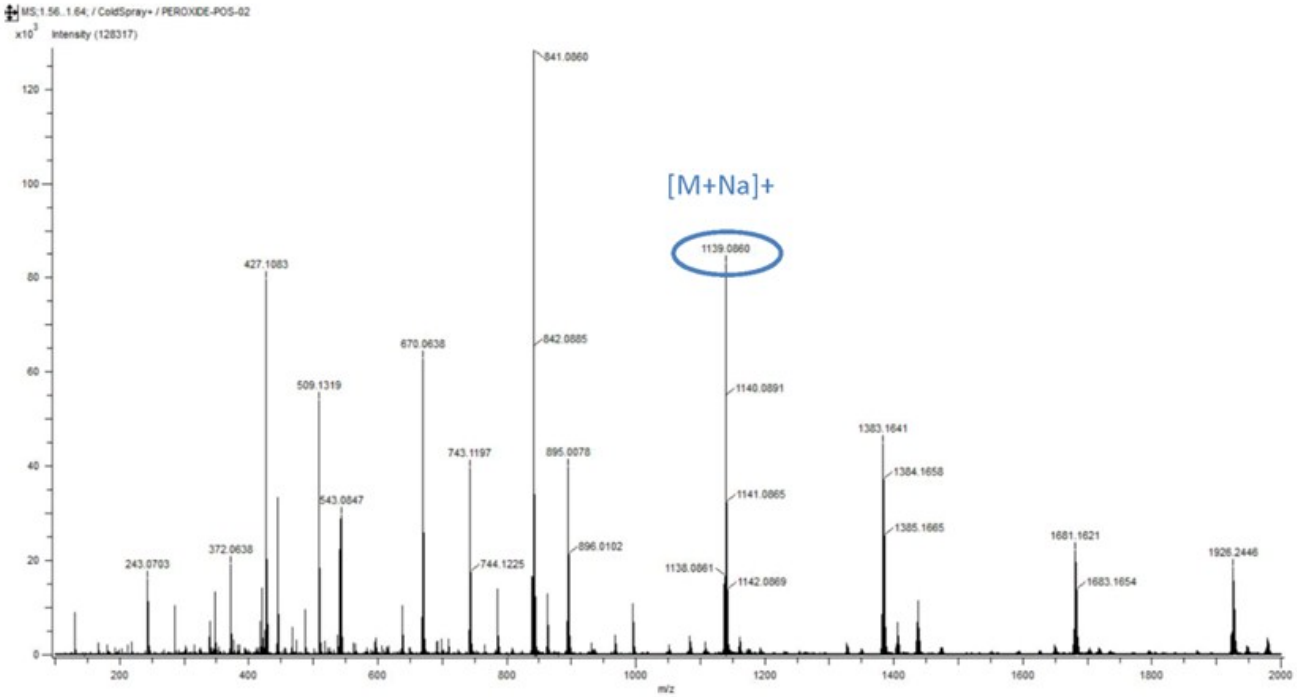

Figure S9. CSI-TOF MS analysis of pure **1** reacted with a slight excess O_2 in DMF at -50 C.

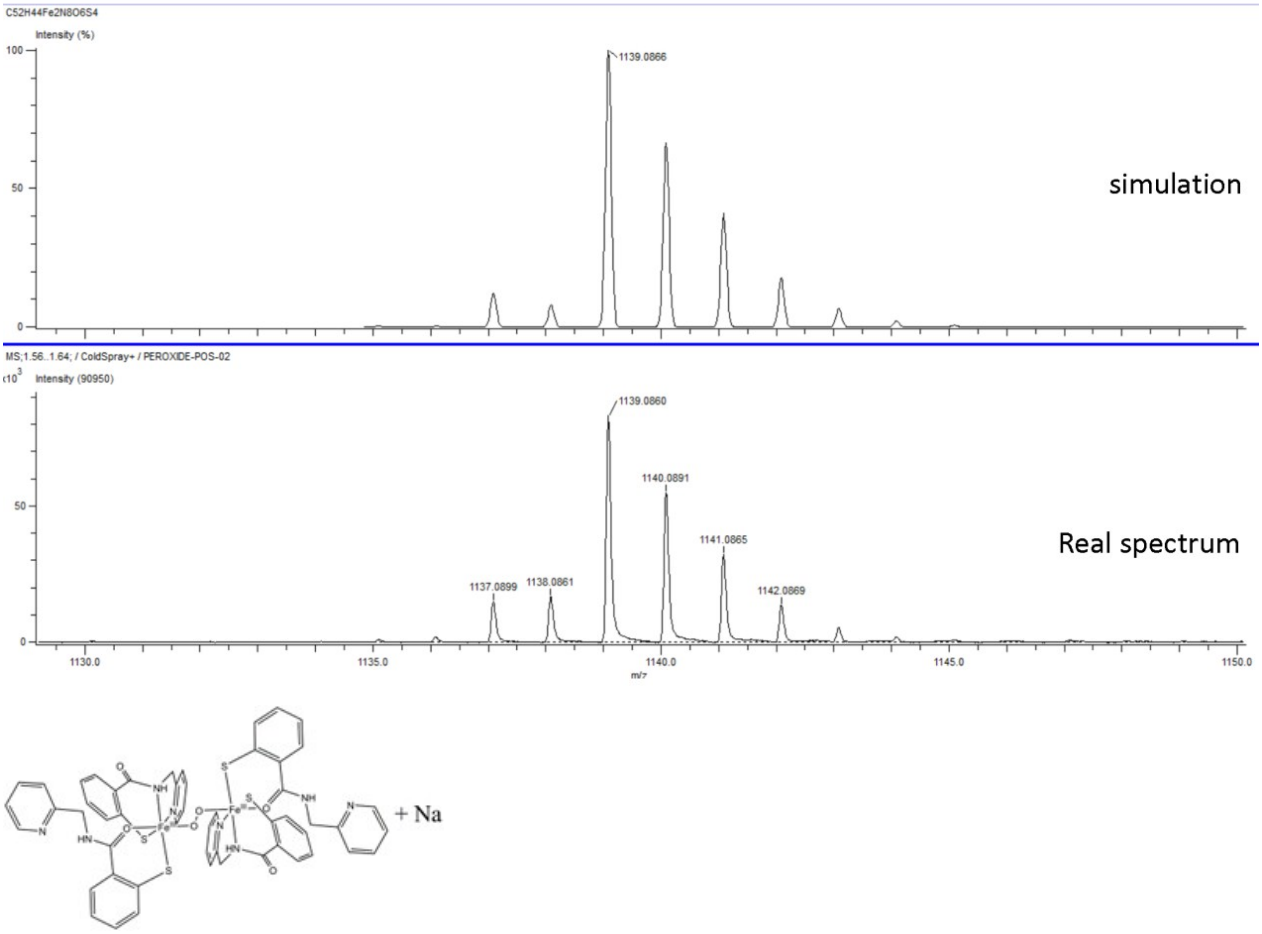

Elemental Composition Estimation

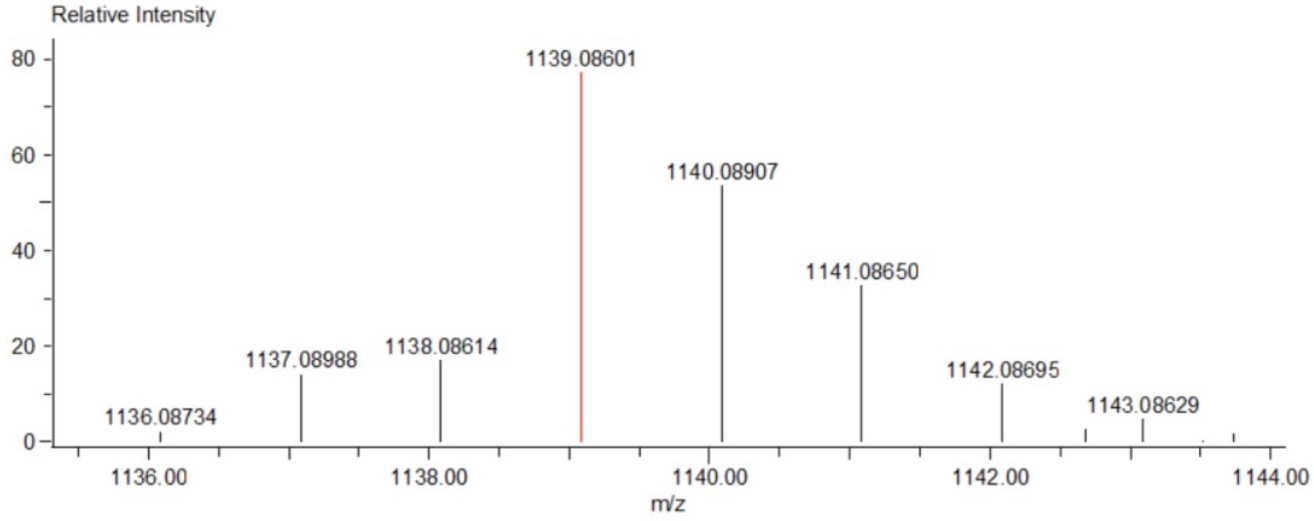

Mass	Calc. Mass	Mass Difference [mDa]	Mass Difference [ppm]	Possible Formula
1139.08601	1139.08632	-0.31	-0.27	$^{12}C_{52}{}^{1}H_{44}{}^{56}Fe_{2}{}^{14}N_{8}{}^{23}Na_{1}{}^{16}O_{6}{}^{32}S_{4}$

Figure S10. The HRMS data along with isotopic distribution pattern of Fe^{III}-O_2-Fe^{III} complex with the composition of [**1** + O_2 + Na]$^+$.

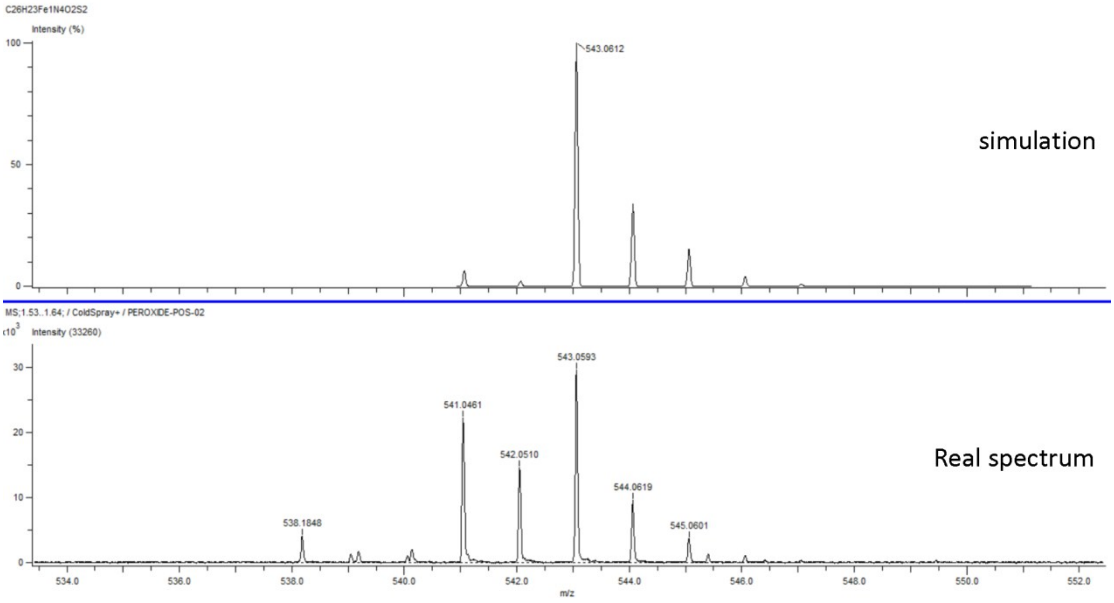

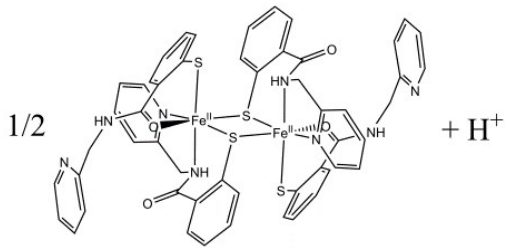

Elemental Composition Estimation

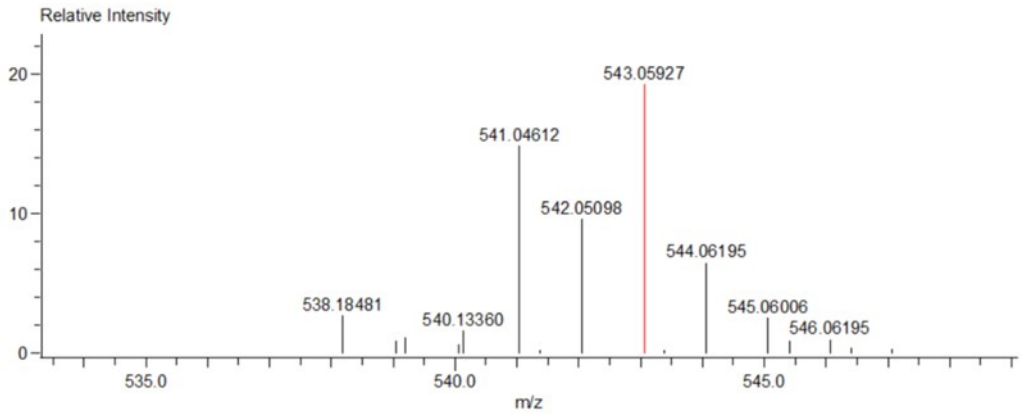

Mass	Calc. Mass	Mass Difference [mDa]	Mass Difference [ppm]	Possible Formula
543.05927	543.06118	-1.92	-3.53	$^{12}C_{26}{}^{1}H_{23}{}^{56}Fe_{1}{}^{14}N_{4}{}^{16}O_{2}{}^{32}S_{2}$

Figure S11. The HRMS data along with isotopic distribution pattern of monomeric **1** complex with the composition of $[0.5\times\mathbf{1} + H]^+$.

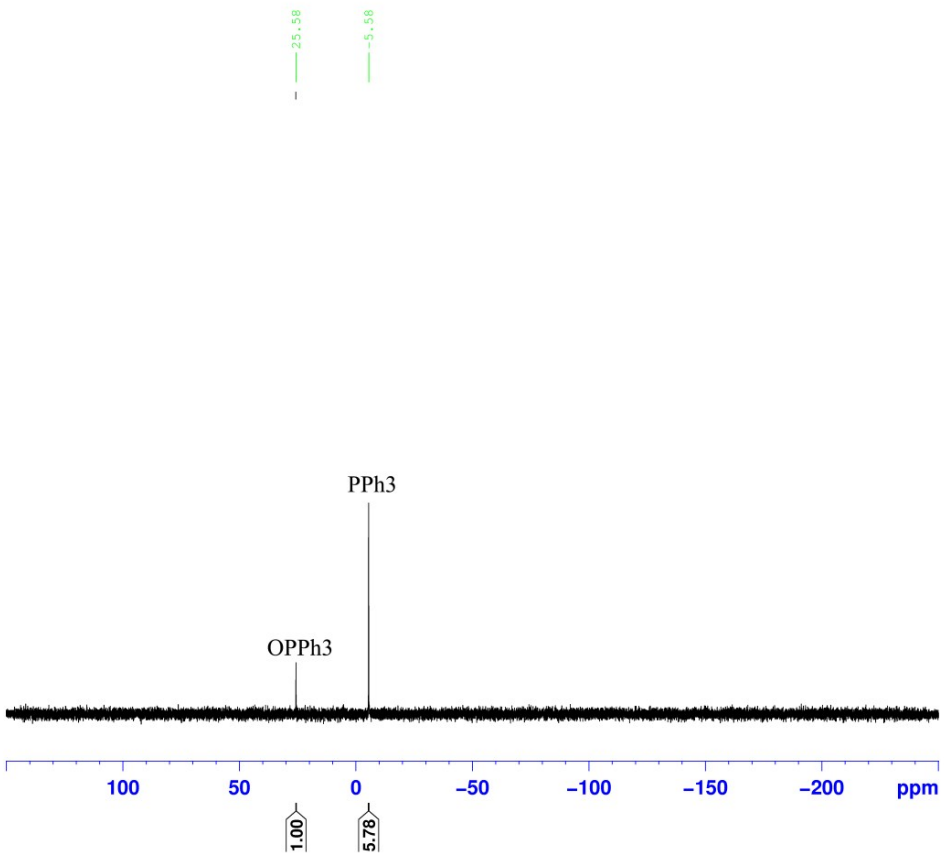

Figure S12. $^{31}P\{^{1}H\}$ NMR spectrum at 298 K. Four equiv. PPh_3 was added to complex **1** in DMF, and then the solution was exposed to air for 20 mins.

```
23-S1-APCI-H#1-20 RT: 0.00-0.28 AV: 20
T: FTMS + p APCI corona Full ms [100.00-2000.00]
m/z=  172.0345-185.4797
Isotope  Min   Max
C-12       0    14
H-1        0    20
Charge 1
Mass tolerance 140.00 ppm
Nitrogen rule not used
RDB equiv -1.00-100.00
max results 1
```

m/z	Intensity	Relative	Theo. Mass	Delta (ppm)	Composition
179.0852	17263.3	100.00	179.0855	-1.61	$C_{14}H_{11}$

Figure S13. HRMS of anthracene for hydride-transfer reaction. 9, 10-dihydroanthracene was added to complex **1** in DCM, and the solution was exposed to air for 30 mins.

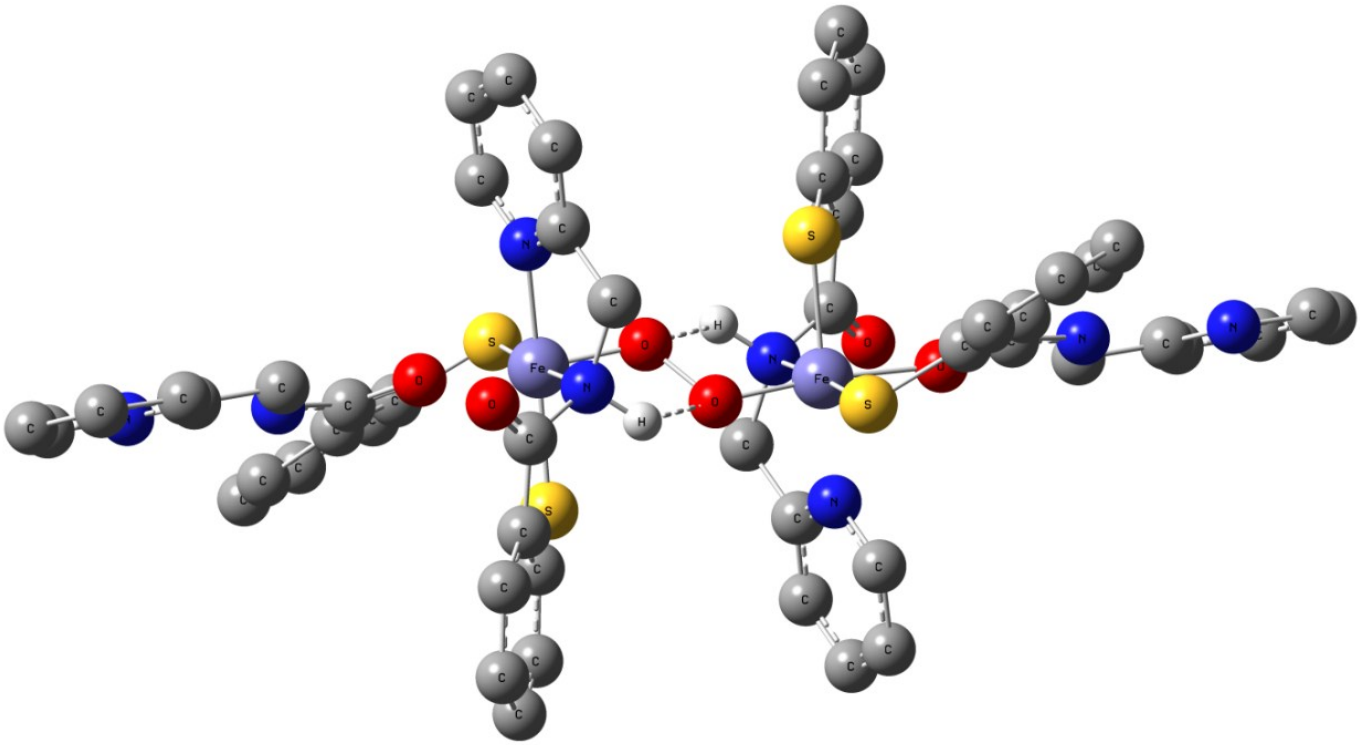

Figure S14. The intramolecular hydrogen bond interactions of the intermediate with **end-on** conformation (**A**) by DFT calculation. The N-O and N-H···O bond distances are 2.69 Å and 1.92 Å, respectively. The other hydrogens were omitted for clarity.

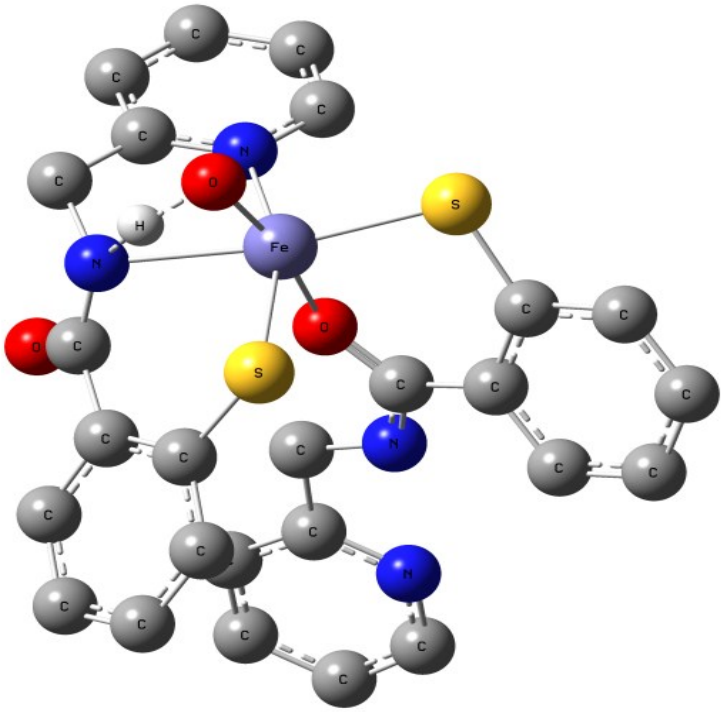

Figure S15. Ball- and stick-type drawings of the transition state **TS**. Some hydrogen atoms are omitted for clarity.

References

1. P. Ghosh, A. Begum, E. Bill, T. Weyhermüller and K. Wieghardt, *Inorg. Chem.*, 2003, **42**, 3208-3215.
2. G. Musie, C.-H. Lai, J. H. Reibenspies, L. W. Sumner and M. Y. Darensbourg, *Inorg. Chem.*, 1998, **37**, 4086-4093.
3. D. K. Mills, Y. M. Hsiao, P. J. Farmer, E. V. Atnip, J. H. Reibenspies and M. Y. Darensbourg, *J. Am. Chem. Soc.*, 1991, **113**, 1421-1423.
4. W.-J. Hu and S. J. Lippard, *J. Am. Chem. Soc.*, 1974, **96**, 2366-2372.
5. D. Sellmann, J. Utz and F. W. Heinemann, *Inorg. Chem.*, 1999, **38**, 459-466.
6. D. Sellmann, Kai P. Peters and Frank W. Heinemann, *Eur. J. Inorg. Chem.*, 2004, **2004**, 581-590.